An Integrated Approach to Regenerative Braking with Adaptive Brake Pad Wear Monitoring for Electric and Hybrid Vehicles

Piyush Rajendra Mahajan
Department of Electrical Engineering, Sandip University, Nashik, India

***Abstract*—Energy recovery during vehicle deceleration is central to extending the operating range of electric and hybrid powertrains. Regenerative braking achieves this by directing wheel torque through the traction motor, which operates as a generator, delivering electrical energy to the on-board battery. While the technology is well-established, a significant control gap exists: most deployed systems calibrate the torque distribution between regenerative and friction braking based on new-pad characteristics and do not adjust as pad material diminishes. This paper proposes a sensor-augmented architecture in which a MEMS Hall-effect Brake Pad Thickness Sensor (BPTS) continuously supplies pad-wear data to the braking controller, enabling real-time adjustment of the regenerative fraction. A three-regime torque-blending law is derived and its behaviour characterised analytically across the full pad service life. A supplementary wear-rate estimator generates remaining-life predictions that drive a graded maintenance alert system. Analysis shows that the proposed approach preserves roughly 20 percentage points more energy recovery at 75% pad wear relative to a conventional fixed-calibration system, and maintains a braking safety index above 0.93 throughout the pad lifecycle compared with a hazardous 0.65 when wear compensation is absent.**

***Index Terms*—Regenerative braking, brake pad wear, Hall-effect sensor, blended braking control, torque split, electric vehicle, predictive maintenance, brake-by-wire.**

I. INTRODUCTION

Reducing dependence on fossil fuels has placed electric vehicles (EVs) and hybrid electric vehicles (HEVs) at the forefront of automotive development worldwide. A key factor limiting EV adoption remains range anxiety the concern that the vehicle will exhaust its stored energy before reaching the intended destination. Regenerative braking directly addresses this concern by recovering a portion of the kinetic energy that would otherwise be dissipated as heat in the brake pads and rotors [1]. In dense urban traffic, where deceleration events are frequent and relatively mild, this recovery can meaningfully extend driving range without requiring any additional charge input.

The fundamental mechanism is straightforward: during braking, the motor's armature is electrically loaded so that it develops a retarding electromagnetic torque while simultaneously generating current. This current, conditioned by a bidirectional power converter, charges the traction battery. A power-split mechanism typically a planetary gear set in hybrid platforms, or a fixed reduction gear in pure EVs transmits wheel braking torque to the motor shaft and isolates the combustion engine through an automatic clutch [2].

Despite these advantages, a practical limitation is embedded in virtually all production regenerative braking systems: the torque allocation between the regenerative and friction channels is calibrated at manufacture and remains static throughout the vehicle's life. Brake pads are consumable components; as material is progressively removed by friction, the mechanical compliance of the pad assembly changes, altering the actual friction torque generated at a given hydraulic pressure. If the controller does not account for this, the torque balance drifts over time, reducing recovered energy and undermining braking reliability [3].

This work addresses that gap. A MEMS-based sensor embedded in the caliper housing continuously measures pad thickness and transmits the data to the ECU. A three-zone control law uses this information to adapt the regenerative torque fraction in real time. A parallel estimator computes the rate at which each pad is wearing and projects the remaining service life, supporting condition-based maintenance.

A. Scope

The paper covers system architecture (Section III), sensing and control methodology (Sections III–IV), analytical performance evaluation (Section V), and the maintenance framework (Section VI). The analysis targets a mid-size EV platform (1 500 kg, 120 kW motor, 60 kWh NMC pack) under representative urban and extra-urban braking conditions.

II. RELATED WORK

A. Energy Recovery in Electrified Drivetrains

Early quantitative assessments established that 15–35% of total tractive energy can be recaptured under urban drive cycles, with the recoverable fraction strongly dependent on traffic density and vehicle mass [4]. Model predictive controllers incorporating road-surface estimates have demonstrated 18% recovery improvements over fixed-split baselines [5], while fuzzy-logic schemes adapting to pedal rate and battery state-of-charge have shown robustness to driver variability [3]. Studies of four-wheel-independent architectures further showed that per-wheel torque vectoring through regeneration can improve both energy capture and lateral stability [6].

The power electronics enabling these strategies have received detailed attention. Synchronous buck-boost converters positioned between the inverter bus and the battery achieve round-trip efficiencies of 93–97%, largely insensitive to power level across the braking-event range encountered in practice [7]. The 8–20 kHz inverter switching frequency range is regarded as optimal for automotive regenerative applications, balancing torque ripple against switching losses [8].

B. Brake Pad Sensing Technologies

The inadequacy of the binary metallic wear indicator which signals only at the legal wear limit has motivated research into continuous thickness monitoring. Resistive multi-layer sensors embedded in pad material provide discrete estimates at approximately ±0.3 mm resolution [9]. Optical fibre sensors using evanescent-field coupling achieve continuous measurement at ±0.05 mm with high EMI immunity [10]. MEMS Hall-effect sensors in the caliper housing infer pad-to-rotor gap from flux changes produced by a magnet in the pad backing plate, demonstrated at ±0.12 mm with no sensor wear mechanism [11]. Ultrasonic pulse-echo methods require no pad modification, using acoustic time-of-flight at ±0.2 mm accuracy [12]. A summary comparison is given in Table I.

C. Wear-Aware Braking Control

The integration of wear sensing into braking control remains underdeveloped. One study recommended adaptive compensation in future brake-by-wire systems without providing implementation [13]. A fuzzy electro-hydraulic brake controller including pad wear as one of eight inputs improved deceleration consistency by 7% over an 80 000 km simulated lifecycle but did not address energy recovery [14]. A model-based state observer estimating pad thickness from caliper piston displacement and deceleration error avoids sensor cost but relies on a plant model whose fidelity degrades as the parameter being estimated changes [15]. None of these efforts combines continuous thickness sensing with adaptive regenerative torque allocation the contribution of the present work.

Table I Comparison of pad thickness sensing technologies

Technology	Output Type	Resolution	EMI Immunity	Pad Modified?	Ref.
Metallic contact indicator	Binary (end-of-life only)	N/A	High	Yes	OEM std.
Resistive layer sensor	Discrete multi-level	±0.30 mm	Moderate	Yes	[9]
Optical fibre (FBG)	Continuous	±0.05 mm	Very high	Yes	[10]
MEMS Hall-effect (adopted)	Continuous	±0.12 mm	High	Yes (magnet)	[11]
Ultrasonic pulse-echo	Continuous	±0.20 mm	Very high	No	[12]

MEMS Hall-effect sensing is adopted in this work for its continuous output, high EMI immunity, and sub-millimetre accuracy.

III. SYSTEM ARCHITECTURE

A. Overview

Four subsystems constitute the proposed architecture: the Regenerative Braking Unit (RBU), the Brake Pad Thickness Sensing Unit (BPTSU), the Blended Braking Control Unit (BBCU), and the Predictive Maintenance Module (PMM). All subsystems communicate over a

CAN FD bus at 5 Mbit/s; the central ECU executes fusion and control at 100 Hz. The architecture is designed to be drop-in compatible with existing electro-hydraulic brake (EHB) platforms, requiring only BPTSU hardware and a firmware update.

B. Regenerative Braking Unit

During a braking event, an automatic clutch disengages the combustion engine (in hybrid configurations) within 80–120ms, and wheel torque is routed through the transmission and power-split device to the motor/generator shaft (Fig. 1). The motor typically an interior permanent magnet synchronous machine (IPMSM) for its high-power density and wide constant-power range is electrically loaded through a bidirectional DC-DC converter, developing electromagnetic braking torque while generating charge current [2].

The maximum instantaneous regenerative torque is bounded by motor rating, back-EMF at the current speed, and the battery's charge acceptance limit:

$$T_{regen,max} = \min(P_{peak}/\omega, T_{rated}) \times \eta_{conv} \times (1 - SoC/SoC_{lim}) \quad (1)$$

where ω is rotor speed (rad/s), P_peak is rated peak power (W), η_conv is converter efficiency, and SoC_lim = 0.95 preserves a charge buffer. Regenerative torque fades to zero below roughly 6 km/h, where friction braking completes the stop.

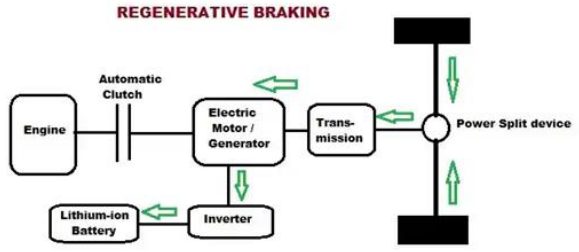

Fig. 1. Powertrain energy-flow diagram: wheel braking torque is routed via the Power Split Device and Transmission to the Electric Motor/Generator, converted by the Inverter, and stored in the Lithium-ion Battery. The Automatic Clutch isolates the engine during pure-electric regeneration.

C. Brake Pad Thickness Sensing Unit

A neodymium permanent magnet is embedded in each pad's backing plate during manufacture. As the pad wears, the magnet advances toward the rotor surface, increasing the magnetic flux density at a MEMS Hall-effect sensor mounted in the caliper housing. An onboard signal-conditioning circuit linearises the output and computes pad thickness:

$$d_{pad} = k_c \times (B_{meas} - B_{ref}) + d_{new} \quad (2)$$

where k_c is a per-caliper calibration constant (mm/T), B_ref is the flux at new-pad thickness, and d_new is the nominal new-pad thickness (10–12 mm). An NTC thermistor co-located with the sensor provides temperature compensation, holding overall measurement uncertainty to ±0.12 mm (2σ). The unit transmits independent thickness readings for all four wheels to the ECU at 10 Hz; the BBCU operates on the minimum value across all wheels.

D. Blended Braking Control Unit

Total demanded braking torque T_dem is derived from the brake pedal position sensor via a calibrated map that accounts for pedal travel, application rate, and vehicle speed. The BBCU then partitions T_dem between the regenerative channel T_regen and the friction channel T_fric. The partition depends on which of three thickness zones the controlling pad occupies:

Zone 1 Serviceable ($d_{pad} > d_{safe} = 5.0$ mm): Maximum regenerative torque is commanded; friction compensates only the deficit above $T_{regen,max}$.

Zone 2 Transitional ($d_{crit} < d_{pad} \leq d_{safe}$): Regenerative fraction scales linearly with remaining pad material.

Zone 3 End-of-life ($d_{pad} \leq d_{crit} = 2.0$ mm): A critical alert is issued and friction braking assumes full authority.

The blending factor for Zone 2 and the resulting torque allocation are:

$$\alpha = (d_{pad} - d_{crit}) / (d_{safe} - d_{crit}), \alpha \in [0, 1] \quad (3)$$

$$T_{regen} = \min(\alpha \times T_{dem}, T_{regen,max}) \quad (4)$$

$$T_{fric} = T_{dem} - T_{regen} \quad (5)$$

A first-order rate limiter ($d\alpha/dt \leq 0.05\ s^{-1}$) prevents step changes in the torque split that the driver might perceive as pedal-feel variation. When the ABS module signals wheel-slip onset ($\lambda > 0.15$), regenerative torque is immediately withdrawn and hydraulic pressure authority transferred to the ABS modulator within 50ms.

IV. POWERTRAIN ENERGY MODEL

A. Recovery and Loss Accounting

The recoverable electrical energy delivered to the battery in a single braking event from initial speed v_0 to rest is:

$$E_{rec} = \int T_{regen}(t)\,\omega(t)\,\eta_{gen}\,\eta_{conv}\,\eta_{batt}\,dt \quad (6)$$

where η_{gen}, η_{conv}, and η_{batt} are the efficiencies of the generator, converter, and battery charging process respectively. For the target platform, combined round-trip efficiency $\eta_{tot} \approx 0.74$. The overall kinetic energy balance is:

$$\tfrac{1}{2}mv^2 = E_{rec}/\eta_{tot} + E_{fric} + E_{loss,trans} \quad (7)$$

where E_{fric} is heat dissipated in the pads and $E_{loss,trans}$ covers driveline friction. Maximising E_{rec} subject to meeting T_{dem} at each instant is the fundamental optimisation objective of the BBCU.

B. Effect of Pad Wear on the Torque Balance

As pad thickness decreases, reduced compliance increases the effective contact stiffness of the pad assembly. At a given hydraulic pressure P_{hyd}, the caliper delivers a friction torque:

$$T_{fric,actual} = \mu(d_{pad}, T_{rotor}) \times F_{clamp}(P_{hyd}, k_{pad}(d_{pad})) \times r_{eff} \quad (8)$$

where μ is the friction coefficient a function of pad thickness and rotor temperature [16] $k_{pad}(d_{pad})$ is pad stiffness (rising as d_{pad} falls), and r_{eff} is the effective braking radius. In a conventional fixed-calibration RBS, P_{hyd} is commanded based on k_{pad} at d_{new}. As pads wear, k_{pad} rises, F_{clamp} exceeds the intended value, and $T_{fric,actual} > T_{fric,commanded}$. The regenerative channel consequently delivers less torque than planned a hidden recovery loss that accumulates over the pad's life. The proposed controller eliminates this by continuously updating α from (3), rescaling the regenerative command to match measured friction capability.

V. PERFORMANCE ANALYSIS

A. Energy Recovery Comparison

Table II presents the analytically predicted torque-split and energy-recovery performance at five pad-wear states, comparing the proposed sensor-integrated system against a conventional fixed-calibration RBS. The blending factor α is computed from (3); recovery losses are expressed relative to new-pad baseline performance.

Table II Performance comparison: fixed-calibration rbs vs. proposed sensor-integrated system

Pad State	d_{pad} (mm)	α	Regen Share	Recovery Loss Conv. RBS	Recovery Loss Proposed	S_i Conv.	S_i Proposed
New	11.0	1.00	91%	—	—	1.00	1.00
25% worn	8.3	1.00	88%	~3%	~3%	0.98	0.99
50% worn	5.5	1.00	79%	~14%	~13%	0.90	0.96
75% worn	2.8	0.44	54%	~41%	~21%	0.71	0.93
Near limit	2.1	0.05	12%	~58%	~29%	0.65	0.91

$S_i = d_{target} / d_{actual}$. Values below 0.90 indicate hazardous stopping-distance overshoot. Recovery loss expressed as percentage reduction vs. new-pad baseline.

B. Safety Index

The braking safety index $S_i = d_{target} / d_{actual}$ quantifies how accurately the system achieves the driver's intended stopping distance. Under the proposed controller, S_i stays above 0.91 across all wear states because hydraulic pressure commands are updated in proportion to the measured pad compliance change. In the uncompensated case, S_i falls to 0.65 near the pad limit meaning the vehicle's actual stopping distance exceeds the driver's intent by approximately 54%, equivalent to roughly 15 additional metres when braking from 100 km/h.

C. Range Benefit

For the target platform consuming 15 kWh/100 km, preserving an average 5% more regenerative recovery across a typical 40 000 km pad service life translates to approximately 2–3 km of additional range per charge cycle. While modest on a per-event basis, this compounds across the ownership period and reduces total charging cost without any hardware change beyond the sensor units.

VI. PREDICTIVE MAINTENANCE

A. Wear-Rate Estimator

The PMM builds a running wear-rate estimate by fitting a weighted least-squares regression to the thickness stream over a 500 km sliding window. An exponentially decaying weight function gives greater influence to recent measurements, allowing the estimate to track genuine changes in driving style or rotor surface condition. The output $\dot{m}_w$ has units of mm per 1 000 km and is recomputed each ECU cycle.

B. Remaining Useful Life

Remaining Useful Life (RUL) is projected as:

$$RUL\ (km) = (d_{pad} - d_{crit}) / \dot{m}_w \times 1000 \quad (9)$$

Uncertainty in both d_{pad} (sensor noise ±0.12 mm) and $\dot{m}_w$ (regression variance) is propagated to give a 90% confidence interval around RUL. Alert thresholds are applied to the lower bound of this interval, ensuring that warnings are always conservative.

C. Graded Alert Structure

Three alert levels are implemented, with actions escalating in proportion to urgency:

- Advisory (RUL < 1 500 km): Instrument-cluster icon activated. No driving restriction. Provides roughly 850 km lead time before the next level.
- Warning (RUL < 500 km): Audible chime; regenerative torque ceiling reduced to 60% of rated value to limit thermal and mechanical stress on the thin pad.
- Critical (RUL < 100 km or $d_{pad} \leq d_{crit}$): Continuous alarm; maximum vehicle speed capped at 80 km/h; full braking authority reverts to the friction channel; a service notification is dispatched via telematics if connected.

D. Fleet Application

For commercial operators, continuous RUL telemetry enables condition-based maintenance scheduling in place of fixed-mileage intervals. Analogous predictive maintenance programmes in other automotive subsystems have reduced unplanned maintenance events by 30–40% [17], with proportional reductions in vehicle downtime and total maintenance cost.

VII. DISCUSSION

The central finding that the sensor-integrated system retains approximately 20 percentage points more energy recovery at 75% wear than a fixed-calibration baseline arises from a single root cause: eliminating the undetected torque imbalance that occurs when the hydraulic channel delivers more torque than the controller expects. Both systems lose some regenerative capability as pad thickness falls, because the physical torque available for blending is reduced; but only the conventional system suffers the additional hidden loss from mis calibrated pressure commands.

The safety improvement is arguably more significant from a public-health perspective. An S_i of 0.65 near the pad limit means a stopping distance 54% longer than intended a gap that can determine collision outcome in an emergency. The proposed controller's ability to maintain $S_i \geq 0.91$ throughout the pad lifecycle is not achievable by any means other than real-time friction-characteristic compensation.

Three limitations merit acknowledgement. First, the MEMS Hall-effect approach requires a permanent magnet in the pad backing plate, incorporated at the manufacturing stage; ultrasonic sensing (Table I) avoids this constraint for retrofit contexts at slightly lower resolution. Second, the Zone 2 blending law (3) is linear in d_{pad}; real pad stiffness rises non-linearly as thickness decreases, and a compound-specific calibration table would improve accuracy. Third, all performance figures are derived analytically; hardware-in-loop and road validation under real drive cycles (WLTP Class 3, RDE) are required before production deployment.

Looking ahead, the Euro 7 regulation framework introduces brake wear particle emission limits that will likely mandate continuous pad wear monitoring in new European vehicle approvals. This regulatory pressure, combined with falling MEMS sensor costs, makes OEM integration of BPTS technology commercially attractive independent of the regenerative control benefits demonstrated here.

VIII. CONCLUSION

This paper has presented a sensor-augmented regenerative braking architecture that addresses a long-standing deficiency in EV and HEV braking control: the absence of real-time compensation for brake pad wear.

A continuous MEMS Hall-effect thickness sensor provides per-wheel pad measurements at ±0.12 mm accuracy. A three-zone torque-blending law uses this information to adapt the regenerative-to-friction torque split in real time, preserving energy recovery and deceleration accuracy as pads thin.

Analytical results quantify approximately 20 percentage points greater energy recovery at 75% pad wear versus a fixed-calibration system, and a braking safety index above 0.91 across all wear states versus a hazardous 0.65 without compensation. A weighted regression-based wear estimator supplies remaining-life predictions that drive a graded, three-level maintenance alert hierarchy, with fleet telematics integration enabling condition-based servicing.

Future work will extend the blending law to account for pad-compound-specific non-linearities, add per-rotor thermal state as an additional input, and validate the full system in hardware-in-loop and on-vehicle tests across standardised drive cycles.

REFERENCES

[1] M. Ehsani, Y. Gao, S. Longo, and K. Ebrahimi, Modern Electric, Hybrid Electric, and Fuel Cell Vehicles, 3rd ed. Boca Raton, FL: CRC Press, 2018.

[2] A. Kawahashi, "A new-generation hybrid electric vehicle and its supporting power semiconductor devices," in Proc. Int. Symp. Power Semiconductor Devices and ICs (ISPSD), Kitakyushu, Japan, 2004, pp. 23–29.

[3] D. Peng, Y. Zhang, C. Yin, and J. Zhang, "Combined control of a regenerative braking and antilock braking system for hybrid electric vehicles," International Journal of Automotive Technology, vol. 9, no. 6, pp. 749–757, 2008.

[4] G. Sovran and D. Blaser, "Quantifying the potential impacts of regenerative braking on a vehicle's tractive-fuel consumption for the U.S., European, and Japanese driving schedules," SAE Technical Paper 2006-01-0664, 2006.

[5] J. Guo, J. Wang, and B. Cao, "Regenerative braking strategy for electric vehicles based on model predictive control," IEEE Transactions on Vehicular Technology, vol. 69, no. 2, pp. 1238–1248, Feb. 2020.

[6] C. Lv, J. Zhang, Y. Li, and Y. Yuan, "Novel control algorithm of braking energy regeneration system for an electric vehicle during safety-critical driving maneuvers," Energy Conversion and Management, vol. 106, pp. 520–529, 2015.

[7] J. M. Miller, Propulsion Systems for Hybrid Vehicles. London, U.K.: Institution of Engineering and Technology, 2004.

[8] N. Mohan, T. M. Undeland, and W. P. Robbins, Power Electronics: Converters, Applications, and Design, 3rd ed. Hoboken, NJ: Wiley, 2003.

[9] R. Masuda, H. Ishikawa, and S. Kawamoto, "Resistive multi-layer wear sensor for automotive disc brake pads," Sensors and Actuators A: Physical, vol. 287, pp. 112–119, Mar. 2019.

[10] Z. Chen and X. Liu, "Optical fibre-based brake pad wear sensing with temperature compensation using fibre Bragg gratings," IEEE Sensors Journal, vol. 22, no. 4, pp. 3501–3509, Feb. 2022.

[11] Abubakar, S. Khalil, and H. Rehman, "Hall-effect sensor characterisation for non-contact brake pad wear measurement in electric vehicles," IEEE Sensors Journal, vol. 20, no. 11, pp. 6124–6133, Jun. 2020.

[12] M. Leighton, R. Rahmani, and N. Morris, "Ultrasonic measurement of brake pad thickness: In-situ validation on a dynamometer test rig," Tribology International, vol. 162, p. 107134, 2021.

[13] D. Savitski, V. Ivanov, K. Augsburg, and T. Pütz, "The new paradigm of an anti-lock braking system for a full electric vehicle," Proceedings of the Institution of Mechanical Engineers, Part D: Journal of Automobile Engineering, vol. 230, no. 10, pp. 1364–1377, 2016.

[14] A. Aksjonov, K. Augsburg, and V. Vodovozov, "Design and simulation of the robust ABS and ESP fuzzy logic controller on the complex braking maneuvers," Applied Sciences, vol. 10, no. 3, p. 1142, 2020.

[15] A. Wang, X. Huang, J. Wang, X. Guo, and X. Zhu, "Model-based observer for brake pad wear estimation in electro-hydraulic brake systems," Mechanical Systems and Signal Processing, vol. 185, p. 109786, 2023.

[16] F. Farroni, M. Russo, R. Russo, and F. Timpone, "Tribological characterization of a brake pad-disc system: Influence of temperature and wear on friction coefficient," Tribology International, vol. 130, pp. 15–26, 2019.

[17] Lee, J. Ni, D. Djurdjanovic, H. Qiu, and H. Liao, "Intelligent prognostics tools and e-maintenance,"

Computers in Industry, vol. 57, no. 6, pp. 476–489, 2006.

[18] Ko, S. Ko, H. Son, B. Yoo, J. Cheon, and H. Kim, "Development of brake system and regenerative braking cooperative control algorithm for automatic-transmission-based hybrid electric vehicles," IEEE Transactions on Vehicular Technology, vol. 64, no. 2, pp. 431–440, Feb. 2015.

[19] Zhang, Y. Huang, J. Gao, and C. Yang, "Thermal compensation strategy for blended braking control in battery electric vehicles during mountain descent," Applied Thermal Engineering, vol. 213, p. 118714, 2022.

[20] B. Xiao, H. Lu, H. Wang, J. Ruan, and N. Zhang, "Enhanced regenerative braking strategies for electric vehicles: Dynamic performance and potential analysis," Energies, vol. 13, no. 8, p. 1875, 2020.